

# Energy budget-based backscatter in an eddy permitting primitive equation model



Malte F. Jansen<sup>a,b,c,\*</sup>, Isaac M. Held<sup>b,c</sup>, Alistair Adcroft<sup>b,c</sup>, Robert Hallberg<sup>b,c</sup>

<sup>a</sup> Department of the Geophysical Sciences, The University of Chicago, Chicago, IL 60637, USA

<sup>b</sup> NOAA Geophysical Fluid Dynamics Laboratory, Princeton, NJ 08540, USA

<sup>c</sup> Program in Atmospheric and Oceanic Sciences, Princeton University, Princeton, NJ 08540, USA

## ARTICLE INFO

### Article history:

Received 15 April 2015

Revised 3 July 2015

Accepted 22 July 2015

Available online 31 July 2015

### Keywords:

Backscatter  
Eddy parameterization  
Mesoscale  
Eddy-permitting  
Energy budget  
Negative viscosity

## ABSTRACT

Increasing computational resources are starting to allow global ocean simulations at so-called “eddy-permitting” resolutions, at which the largest mesoscale eddies can be resolved explicitly. However, an adequate parameterization of the interactions with the unresolved part of the eddy energy spectrum remains crucial. Hyperviscous closures, which are commonly applied in eddy-permitting ocean models, cause spurious energy dissipation at these resolutions, leading to low levels of eddy kinetic energy (EKE) and weak eddy induced transports. It has recently been proposed to counteract the spurious energy dissipation of hyperviscous closures by an additional forcing term, which represents “backscatter” of energy from the un-resolved scales to the resolved scales. This study proposes a parameterization of energy backscatter based on an explicit sub-grid EKE budget. Energy dissipated by hyperviscosity acting on the resolved flow is added to the sub-grid EKE, while a backscatter term transfers energy back from the sub-grid EKE to the resolved flow. The backscatter term is formulated deterministically via a negative viscosity, which returns energy at somewhat larger scales than the hyperviscous dissipation, thus ensuring dissipation of enstrophy. The parameterization is tested in an idealized configuration of a primitive equation ocean model, and is shown to significantly improve the solutions of simulations at typical eddy-permitting resolutions.

© 2015 Elsevier Ltd. All rights reserved.

## 1. Introduction

The ocean circulation is strongly controlled by mesoscale turbulent eddies (e.g. Gill et al., 1974; Johnson and Bryden, 1989; Hallberg and Gnanadesikan, 2006; McWilliams, 2008; Waterman et al., 2011). However, most of the current generation climate models, as for example appeared in the report of the Intergovernmental Panel on Climate Change (IPCC; Flato et al., 2013), have too little spatial resolution to resolve these turbulent motions. The effect of unresolved turbulent motions on the larger-scale resolved flow thus must be parameterized. Since any such parameterization is associated with uncertain assumptions about the properties of the eddies, many modeling groups aim to increase the resolution of their ocean climate models such as to resolve eddies explicitly. In the near future we expect the resolution of many IPCC-class ocean models to be refined to around 1/4 of a degree. These resolutions are often considered “eddy permitting”, because the models produce eddy-like disturbances generated by baroclinic instability of the flow, but the resolution is still

insufficient to properly resolve the mesoscale eddy field (e.g. Hallberg and Gnanadesikan, 2006; Hallberg, 2013). It therefore remains important to devise parameterizations that adequately describe sub-grid eddy effects at these eddy-permitting resolutions.

The qualitative properties of the mesoscale eddy field in the ocean can be understood by considering the quasi-geostrophic (QG) approximation (Charney, 1971; Rhines, 1977; Salmon, 1978). A fundamental property of QG turbulence is the transfer of enstrophy (i.e. vorticity variance) to smaller and smaller scales, by non-linear eddy-eddy interactions (Charney, 1971). In an ocean model where only part of the mesoscale eddy kinetic energy (EKE) spectrum is resolved, enstrophy must be removed near the grid-scale to represent the net transfer of enstrophy to the subgrid-scale, and avoid accumulation. This is commonly achieved by a horizontal hyper-viscosity—typically bi-harmonic (i.e. fourth order)—which scale-selectively removes enstrophy near the grid-scale (e.g. Böning and Budich, 1992; Griffies and Hallberg, 2000; Oschlies, 2002; Fox-Kemper and Menemenlis, 2008). However, at “eddy permitting” resolutions, where the grid-scale is on the same order as the first baroclinic deformation radius, such closures dissipate not only enstrophy, but also a significant amount of energy (e.g. Jansen and Held, 2014). This energy dissipation is not desired, since QG turbulence generally does not transfer energy to

\* Corresponding author at: Department of the Geophysical Sciences, The University of Chicago, Chicago, IL 60637, USA. Tel.: +1 617 230 0262.

E-mail address: [mfj@uchicago.edu](mailto:mfj@uchicago.edu) (M.F. Jansen).

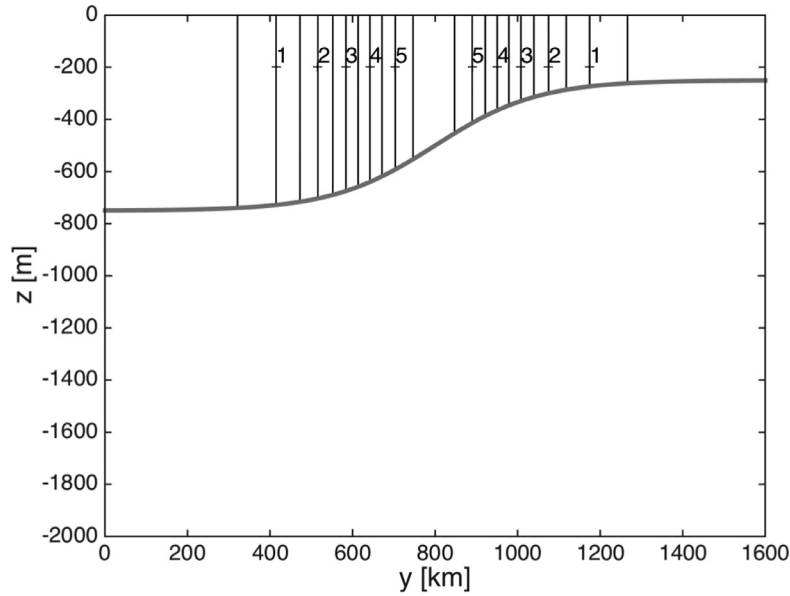


**Fig. 1.** Interface height (thick grey line) and associated geostrophic velocity (black contours—contour interval: 0.5 cm/s) for the equilibrium solution of the interface-height restoring forcing. Notice that, in the absence of horizontal momentum fluxes (required to balance frictional drag in the vertically integrated zonal mean zonal momentum budget), there is no flow in the lower layer.

smaller scales in the net, and thus does not provide a pathway to energy dissipation at small scales. As a result of this spurious viscous energy dissipation, eddy-permitting models typically have too little EKE and too weak eddy induced transports (e.g. Hallberg, 2013; Jansen and Held, 2014; Griffies et al., 2015).

Jansen and Held (2014) recently proposed to combine a hyperviscous closure with a forcing term, which is chosen such as to cancel the spurious energy dissipation associated with the hyperviscosity, while maintaining a net dissipation of enstrophy. A similar approach has also been proposed independently by Thuburn et al. (2014), who show improvements in simulations of barotropic turbulence. The forcing term may be thought of as representing back-scatter of kinetic energy from the subgrid scales to the resolved flow (see e.g. Kraichnan, 1976; Leith, 1990; Frederiksen and Davies, 1997; Duan and Nadiga, 2007; Kitsios et al., 2013; Grooms et al., 2015; Berloff, 2015). Jansen and Held (2014) test two different formulations for the backscatter term in a two-layer QG model, one stochastic and one deterministic. Either approach is shown to greatly improve the results of simulations at eddy permitting resolutions.

In this paper we formulate a parameterization based on the argument of Jansen and Held (2014) for a primitive equation ocean model. The main additions to the results discussed in Jansen and Held (2014) are the implementation in a primitive-equation finite-volume model (the simulations in Jansen and Held (2014) employed a QG pseudo-spectral model), as well as the formulation of a local prognostic sub-grid EKE budget, which is necessary to adequately account for spatial inhomogeneities in the eddy field. The backscatter from the sub-grid EKE to the resolved flow will be formulated similarly to the deterministic approach in Jansen and Held (2014) using a negative Laplacian viscosity. A similar approach has also been found to be successful in the barotropic turbulence simulations of Thuburn et al. (2014), and is supported by the theoretical results of Kraichnan (1976) and Galperin et al. (1993).

## 2. Resolution dependence of numerical simulations

In the following section we discuss results from a series of numerical simulations, using an idealized two-layer configuration of the GOLD ocean model (Hallberg, 2013; Hallberg and Adcroft, 2009). The model setup is described in Section 2.1. In Section 2.2 we discuss properties of the emerging turbulent flow and their dependence

on the horizontal resolution. Consistent with the results of Jansen and Held (2014), simulations at eddy-permitting resolution will be shown to have too little EKE, as well as too weak eddy-driven mean flows. The purpose of the backscatter parameterization, discussed in Section 3, is to alleviate this shortcoming.

### 2.1. Model description

The numerical model setup is based on the two-layer zonally-reentrant channel configuration of the GOLD ocean model discussed by Hallberg (2013), but with added topography and somewhat modified parameters, more typical of the Southern Ocean. The Cartesian-coordinate channel measures 1600 km  $\times$  1600 km, and is bounded meridionally by free slip, no-normal-flow boundary conditions. The Coriolis parameter increases from  $f = 1.1 \times 10^{-4} \text{s}^{-1}$  at the southern end of the domain to  $f = 1.3 \times 10^{-4} \text{s}^{-1}$  at the northern end of the domain. While motivated by the Southern Ocean, our simulations thus represent a northern hemisphere channel flow. The upper layer extends on average over the upper 500 m of the 2000 m deep domain. The zonal mean interface height is restored to a hyperbolic tangent profile with a characteristic width of 500 km, on a time-scale of one year, but with no damping of departures from the zonal mean. The equilibrium solution for the interface height restoring is shown in Fig. 1. The density contrast between the two vertical layers is  $\delta\rho/\rho_0 = 7 \times 10^{-4}$ , leading to a baroclinic gravity wave speed of about  $\sqrt{\delta\rho/\rho_0 g H_1 H_2 (H_1 + H_2)^{-1}} \approx 1.6 \text{ ms}^{-1}$ . The bottom topography consists of an interrupted meridional ridge and a seamount (Fig. 2). The maximum topographic elevation is 750 m, which is about half of the lower layer depth. Bottom friction is described via a quadratic drag law, with a bottom-drag coefficient  $C_D = 0.03$ . An additional background bottom velocity,  $U_0 = 0.1 \text{ m/s}$ , is included in the computation of the bottom drag, as a crude representation of tidal currents and other missing processes in the deep ocean. Enstrophy is dissipated near the grid-scale using a biharmonic viscosity, with a viscosity coefficient following Smagorinsky (1963) (see Griffies and Halberg, 2000, for the biharmonic formulation):

$$\nu_4 = C_{\text{Smag}} \Delta^4 |D|. \quad (1)$$

$C_{\text{Smag}}$  here is a constant non-dimensional coefficient,  $\Delta$  is the grid-spacing, and  $|D| = \sqrt{(u_x - v_y)^2 + (u_y + v_x)^2}$  is the deformation rate.

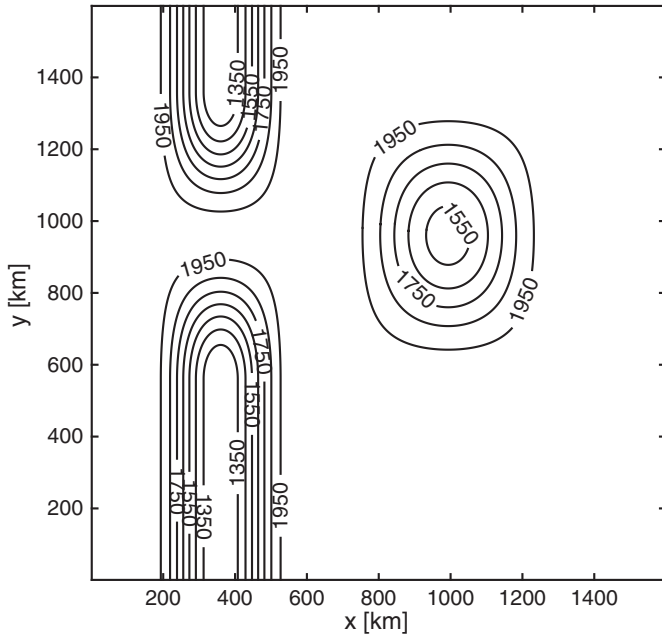


Fig. 2. Model bathymetry (depth in m—contour interval: 100 m).

Unless otherwise noted, the Smagorinsky coefficient is chosen similarly as in GFDL’s global ocean models:  $C_{\text{Smag}} = 0.06$ . The sensitivity of the results to  $C_{\text{Smag}}$  will be discussed.

The non-linear advection of momentum in the model is formulated in terms of a vorticity flux (or generalized Coriolis) term and a KE gradient term (Hallberg, 2013). Of particular importance here is the representation of the vorticity flux term, whose discretization impacts the models conservation properties for kinetic energy and enstrophy. Since the energy and enstrophy budget lies at the core of the developed parameterization, it is desirable to choose a numerical discretization which by itself is approximately conservative. The numerical discretization used for this study is based on a formulation discussed in Arakawa and Hsu (1990). This scheme exactly conserves energy and conserves enstrophy in the limit that the horizontal mass flux is non-divergent.

The baroclinic deformation radius varies from about 9 km at the northern end of the domain and above the topography, to about 16 km at the southern end of the domain. Using a similar setup (though without bottom topography), Hallberg (2013) argued that the grid-spacing may be at most half as large as the deformation radius to adequately resolve baroclinic eddies. Simulations are here performed at varying resolutions between  $\Delta = 3.2$  km and  $\Delta = 20$  km. While  $\Delta = 3.2$  km is expected to be adequately eddy resolving,  $\Delta = 20$  km may be considered barely eddy permitting, as the grid-spacing exceeds the baroclinic deformation radius. All simulations are spun-up to a statistical equilibrium for 15 years, and flow statistics are averaged for 15 years following this initial spin-up period.

## 2.2. Resolution dependence

Figs. 3 and 4 show the time-mean flow and EKE for simulations at 3.2 km, 10 km, and 20 km resolution. The highest resolution (3.2 km) reference simulation shows an overall eastward flow in the upper layer which is strongly channeled by the topographic features shown in Fig. 2. The flow around topography is generally anti-cyclonic, which becomes particularly clear in the lower level, where the flow is dominated by an anti-cyclone centered above the sea mount near  $y = 1000$  km. Additional localized currents emerge near the edges of the ridge around  $y = 200 - 600$  km. The spin-up of anti-cyclonic flows around sea-mounts is commonly known as the “Neptune effect”, and is caused by eddy PV fluxes acting to reduce

the PV anomaly associated with the topography (Bretherton and Haidvogel, 1976; Holloway, 1992; Greatbatch and Li, 2000). Strong EKE is found mostly between about  $y = 500$  km and  $y = 1300$  km. It is largest down-stream of the topographic features—particularly in the lee of the sea mount—and weaker right above the topography.

At a resolution of  $\Delta = 10$  km the EKE is significantly reduced, though the overall spatial pattern remains largely similar. Changes in the mean flow are larger in the lower layer, which shows a weakening of the topographically induced flow. Since this flow is driven by eddy fluxes of PV, the weakening of the topographic mean flow is expected as a result of the reduced EKE. At  $\Delta = 20$  km the EKE is much too weak, resulting in weak topographically steered flows in the lower layer. Changes in the upper layer mean flow are less dramatic, but the flow becomes significantly more zonally symmetric, and more confined to the region between  $y \approx 400$  km and  $y \approx 1200$  km, thus more closely resembling the equilibrium solution of the restoring (Fig. 1).

Additional simulations were performed at horizontal resolutions of 5 km and 32 km (not shown). The results obtained at 5 km resolution differ relatively little from those at 3.2 km resolution, suggesting that the large-scale flow field is mostly converged at this resolution. This is in agreement with the numerical results of Hallberg (2013), as well as with the theoretical discussion in Jansen and Held (2014), which concluded that spurious hyper-viscous energy dissipation decreases rapidly when the grid-scale becomes small compared to the deformation radius. At 32 km resolution, eddies are absent and the mean flow is virtually identical to the equilibrium solution of the restoring.

An important role of eddies in the ocean is to drive an overturning transport, which releases available potential energy from the mean state (and thus acts as the source of energy for the eddies themselves) and contributes to the transport of heat and other tracers (e.g. Johnson and Bryden, 1989; Hallberg and Gnanadesikan, 2006; McWilliams, 2008). Due to the lack of an explicit wind stress, which would drive an Eulerian circulation, the entire meridional overturning transport in the present model is driven by eddy fluxes. The overturning transport in a statistically steady state can be computed as

$$\Psi \equiv \overline{[v_1 h_1]} = -\overline{[v_2 h_2]}, \quad (2)$$

where the overbar and brackets respectively denote the time- and zonal-average,  $v_i$  is the meridional velocity in layer  $i$ , and  $h_i$  is the layer thickness. Due to the conservation of mass (or volume in the Boussinesq limit), the total transport in the two layers is equal and opposite.

The overturning transport for the three simulations discussed above is shown in Fig. 5 (solid lines). The high resolution reference simulation (black line) shows a meridional overturning transport that is mostly confined to the strongly forced region between about  $y \approx 400$  km and  $y \approx 1200$  km. The overturning transport peaks near the center of the domain at somewhat over  $0.6 \text{ m}^2/\text{s}$ . To get a better appreciation of the magnitude of the overturning transport in our simulations, we can multiply the values in Fig. 5 by the characteristic length of the ACC:  $\approx 20000$  km. This would suggest a peak transport of around 10–15 Sv, which is on the same order as the overturning transport in the ACC (e.g. Talley, 2013). Dividing the overturning transport by the slope of the interface yields an eddy interface height diffusivity, which in turn is analogous to the GM coefficient in  $z$ -coordinate models (e.g. Gent et al., 1995; Hallberg, 2013; Jansen et al., 2015). With a characteristic interface height slope near the domain center of around  $500 \text{ m}/500 \text{ km} = 10^{-3}$ , an overturning transport on the order of  $1 \text{ m}^2/\text{s}$  corresponds to an eddy diffusivity on the order of  $1000 \text{ m}^2/\text{s}$ , which again is on the same order as suggested by observations in the Southern Ocean (e.g. Tulloch et al., 2014).

At a resolution of  $\Delta = 10$  km the peak overturning transport is reduced by about 20% relative to the high resolution simulation. The relative weakening is somewhat stronger on the flanks of the

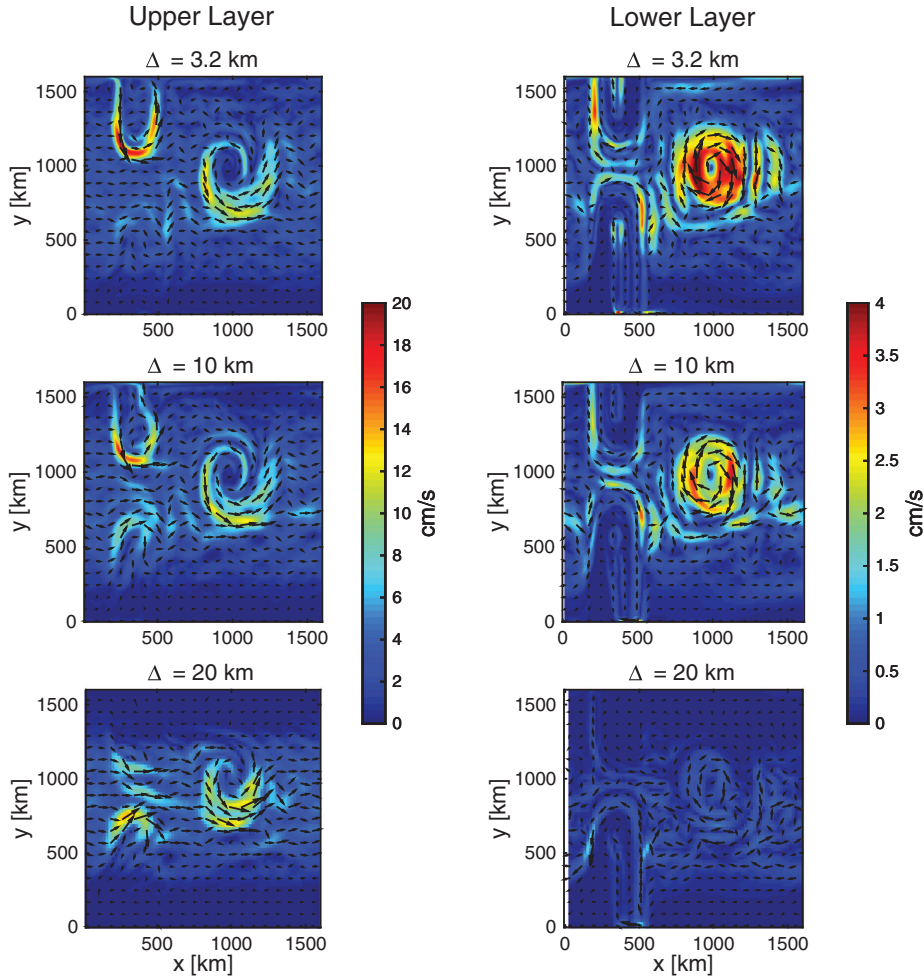


**Fig. 3.** Time-mean flow speed (shading) and direction (arrows) for simulations with 3.2 km (top), 10 km (middle), and 20 km (bottom) resolution. The left column show the mean flow in the upper layer, while the right column shows the mean flow in the lower layer. The color shading is identical between the three simulations, but differs between the two respective vertical layers.

overturning cell, indicating a slight reduction of the meridional extent. At a resolution of  $\Delta = 20$  km, the peak overturning transport is reduced to less than a quarter of the high resolution reference case, and the meridional extent is reduced significantly. The results for the resolution dependence of the overturning transport largely reflect the reduction of EKE observed in Fig. 4.

### 2.2.1. EKE spectra and the role of the Smagorinsky coefficient

To analyze the effect of sub-grid eddy parameterizations, it is often fruitful to look at the EKE budget. For simplicity, we will here focus on the barotropic mode EKE, which arguably is most important for the eddy heat transport and release of available potential energy (e.g. Larichev and Held, 1995; Cessi, 2008; Jansen et al., 2015). The spectra are defined as a function of the total wavenumber as

$$E(K) = \frac{d}{dK} \iint_{k^2+l^2 < K^2} \frac{1}{2} (|\hat{u}_t|^2 + |\hat{v}_t|^2) dk dl, \quad (3)$$

where  $\hat{u}_t$  and  $\hat{v}_t$  are the spectral transforms of the zonal and meridional barotropic velocity fields, respectively. The resulting spectra are shown in Fig. 6, with the solid lines denoting the three simulations discussed above. The high resolution reference simulation shows a peak in the EKE spectrum at around wavenumber 8, corresponding to a wavelength of about 200 km. Below that wavenumber the spectral energy falls off with a slope near  $K^{-3}$  (Charney, 1971). A much steeper drop in EKE is found at wavenumbers higher than about 1/3–

1/2 times the Nyquist wavenumber,  $K_N = \pi/\Delta$ , presumably associated with strong dissipation due to the hyper-viscous closure. A brief flattening of the spectrum is again found at wavenumbers just below the Nyquist frequency, but due to the very small amount of energy at these scales this is unlikely to have any significant effect.

At coarser resolution the EKE level is reduced at all scales, with an overall reduction of about 50% at  $\Delta = 10$  km and at least one order of magnitude at  $\Delta = 20$  km (notice the logarithmic axis). As for the high resolution case, the spectra fall off very steeply at wavenumbers higher than about 1/2–1/3 times the Nyquist wavenumber. The steep decline of spectral energy above the grid-scale suggests a potentially inappropriately large viscosity coefficient. The (bi-harmonic) viscosity coefficient was here formulated following the arguments of Smagorinsky (1963) and Griffies and Halberg (2000), as discussed in Section 2.1. While this formulation is adaptive to changes in the resolution and flow properties, it is defined only to within the non-dimensional constant factor,  $C_{\text{Smag}}$ . The latter was chosen based on experience with global models, where larger viscosities may be desirable either to suppress numerical noise in certain regions (such as western boundary currents) or to reduce the grid Reynolds number in order to minimize numerical diffusion (Ilcak et al., 2012).

To analyze the impact of reduced bi-harmonic viscosity, we repeated the eddy-permitting simulations with  $\Delta = 10$  km and  $\Delta = 20$  km, using a Smagorinsky coefficient reduced by one order of magnitude, i.e.  $C_{\text{Smag}} = 6 \times 10^{-3}$ . The resulting EKE spectra are shown as dotted lines in Fig. 6. As expected, the reduction of the Smagorinsky

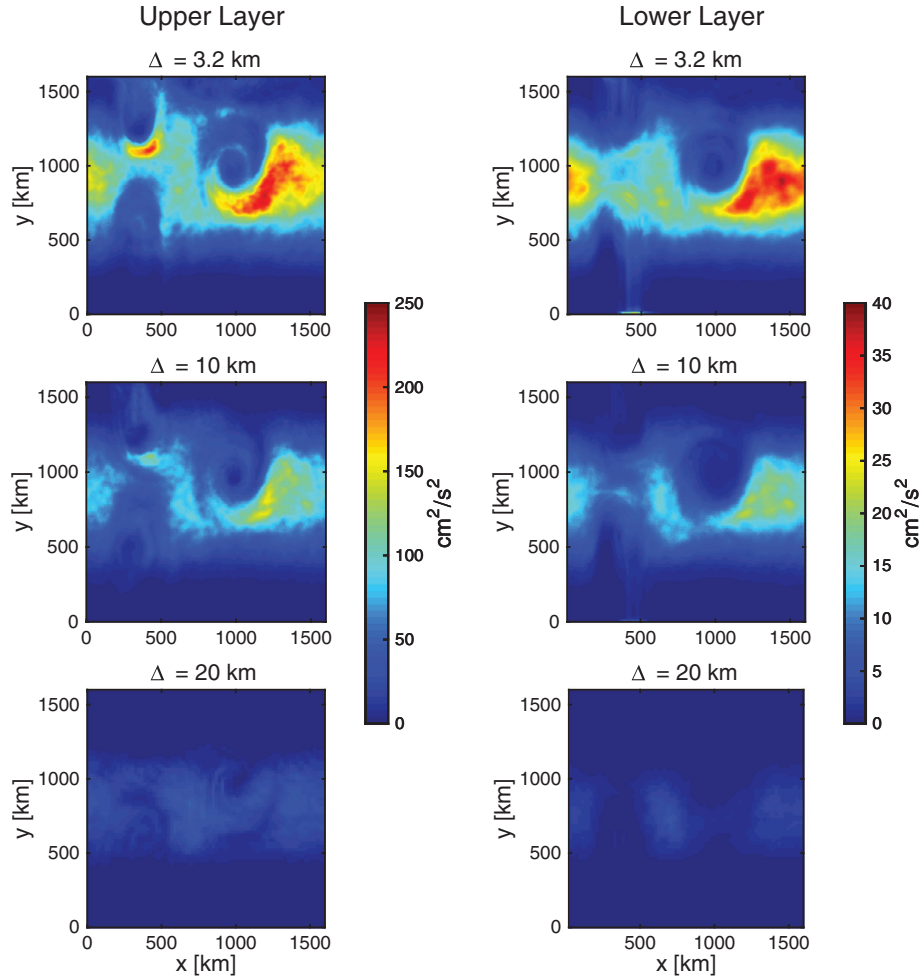


**Fig. 4.** Time-mean EKE for simulations with 3.2 km (top), 10 km (middle), and 20 km (bottom) resolution. The left column show the EKE in the upper layer, while the right column shows the EKE in the lower layer. The color shading is identical between the three simulations, but differs between the two respective vertical layers.

coefficient leads to a considerable increase in EKE near the grid-scale. Moreover, the energy level is increased also at scales much larger than the grid-scale. The increased EKE at larger scales is in agreement with the argument of [Jansen and Held \(2014\)](#), who showed that spurious energy dissipation near the grid-scale leads to reduced EKE levels at all scales by suppressing energy backscatter to larger scales. However, while the EKE levels near the peak of the energy spectrum are increased, they remain about 20% too low for the simulation with  $\Delta = 10$  km and too low by about a factor of five for the simulation with  $\Delta = 20$  km, as compared to the high resolution reference case.

Similar improvements are found with respect to other flow characteristics. The dotted lines in [Fig. 5](#) show the overturning transport for the simulations with reduced  $C_{\text{Smag}}$ . As for the EKE, the overturning transports are increased relative to the simulations with the default Smagorinsky coefficient, but they remain too low as compared to higher resolution simulations. Particularly at a resolution of  $\Delta = 20$  km, the overturning transport remains much too weak. Similar results are also found for the mean flow (not shown).

### 3. An energetically consistent backscatter parameterization

[Jansen and Held \(2014\)](#) argue that the reduction of EKE at eddy-permitting resolutions, and the associated deficiencies in the eddy fluxes and mean flow properties, are primarily a result of spurious EKE dissipation by the viscous closure. While the viscous dissipation of EKE can be minimized by using a high-order hyperviscosity and

a relatively weak hyperviscosity coefficient, the requirement to dissipate a certain amount of enstrophy necessarily implies a certain amount of energy dissipation, for any purely dissipative closure. At eddy permitting resolution (i.e. when the grid scale is on the same order as the Rossby radius of deformation) this spurious energy dissipation represents a significant part of the total EKE generation ([Jansen and Held, 2014](#)). To overcome the problem, [Jansen and Held \(2014\)](#) propose to combine the hyperviscous dissipation with a forcing term that returns energy to the resolved flow, and may be thought of as representing “backscatter” of energy from the sub-grid scale.

The closure presented in [Jansen and Held \(2014\)](#) is based on a global energy budget, and implies an assumption about spatial homogeneity of the flow. This assumption is inappropriate for larger, inhomogeneous domains, such as the global ocean, or even the idealized setup used for this study. We therefore propose to combine the argument of [Jansen and Held \(2014\)](#) with the suggestion of [Eden and Greatbatch \(2008\)](#) to formulate eddy parameterizations based on an explicit predictive sub-grid EKE budget (see also [Cessi, 2008](#); [Marshall and Adcroft, 2010](#); [Jansen et al., 2015](#)). The formulation of the closure is derived in the following [Section 3.1](#), and numerical results are discussed in [Section 3.2](#).

#### 3.1. Formulation

In the numerical model discussed above, enstrophy and energy is dissipated near the grid scale by a bi-harmonic horizontal viscosity. The vertically averaged energy tendency of the resolved flow

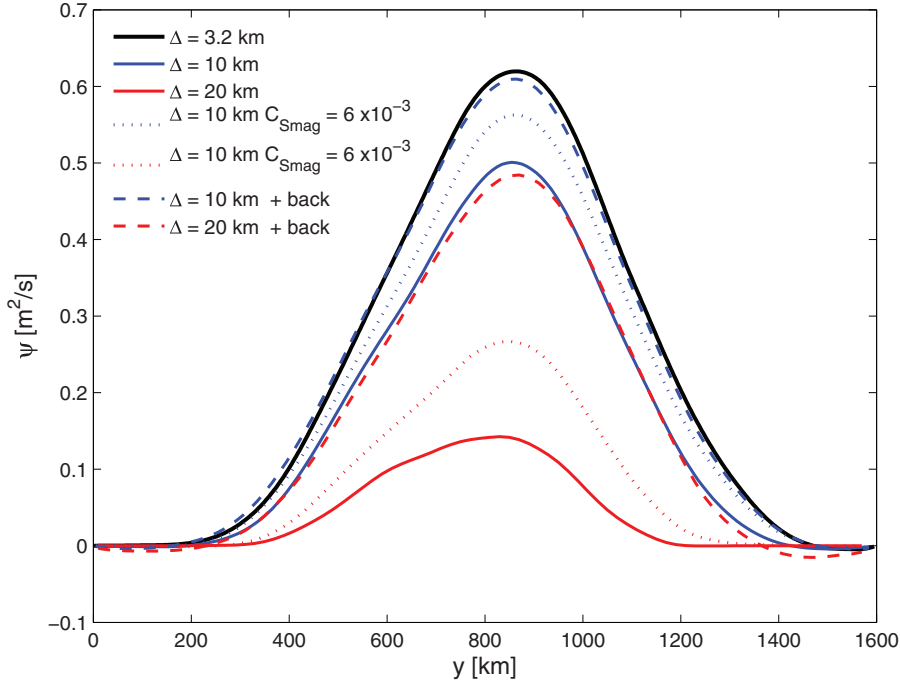


**Fig. 5.** Overturning transport (Eq. (2)) in units of  $\text{m}^2/\text{s}$ . The black line shows the high resolution reference simulation with a grid-spacing  $\Delta = 3.2$  km. Blue lines show simulations with a resolution of  $\Delta = 10$  km, and red lines show simulations with a resolution of  $\Delta = 20$  km. The solid lines show results from the reference simulations with Smagorinsky-type biharmonic viscosity and  $C_{\text{Smag}} = 6 \times 10^{-2}$ . The dotted lines show results from simulations with a reduced Smagorinsky coefficient:  $C_{\text{Smag}} = 6 \times 10^{-3}$  (see Section 2.2.1). The dashed lines show results using the backscatter parameterization discussed in Section 3. (For interpretation of the references to color in this figure legend, the reader is referred to the web version of this article.)

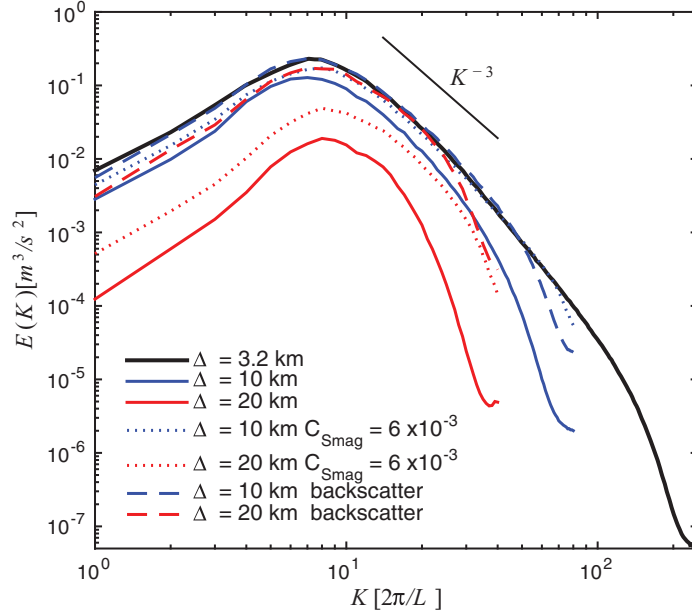


**Fig. 6.** Barotropic EKE as a function of the total wavenumber, normalized by the width of the domain:  $K = (k^2 + l^2)^{1/2} / (2\pi/L)$ . The different simulations are marked as in Fig. 5.

associated with biharmonic dissipation can be computed as

$$\dot{E}_{\text{diss}} = \frac{1}{H} \sum_i h_i A_{h,i} \nabla \mathbf{u}_i \cdot \nabla (\nabla^2 \mathbf{u}_i) \quad (4)$$

where  $h_i$  is the thickness of layer  $i$ ,  $H$  is the total depth, and  $A_{h,i}$  is the biharmonic horizontal viscosity coefficient, which may vary both in the horizontal as well as between vertical layers.  $\mathbf{u}_i$  here denotes the horizontal velocity vector and  $\nabla = (\partial_x, \partial_y)$  the horizontal gradient. For simplicity the equations are here formulated for an isopycnal layer model, and assuming a Cartesian coordinate system, as applies for our idealized model setup. However, the implementation in GOLD

makes use of a generalized coordinate formulation and can thus readily be used in a global model configuration (Griffies and Halberg, 2000; Griffies, 2004). While not strictly negative definite, the term in (4) generally represents a sink of EKE to the resolved flow.

To compensate for the energy loss associated with the biharmonic viscosity, we want to include an additional forcing term in the momentum equation, which may be interpreted as representing backscatter of EKE from the sub-grid scales to the resolved flow. Jansen and Held (2014) propose two formulations for this forcing term: a stochastic “noise” forcing and a (deterministic) negative Laplacian viscosity. Both approaches were shown to be successful,

with the results using negative viscosity being somewhat superior. We therefore adopt the strategy to parameterize backscatter using a negative Laplacian viscosity. While negative viscosity by itself also adds enstrophy to the resolved flow, the proposed (energy conserving) combination of a hyper-viscous dissipation with a negative Laplacian viscosity leads to a net dissipation of enstrophy. Negative viscosity backscatter acts at larger scales than hyper-viscous dissipation, thus leading to a net transfer of energy from the grid-scale to larger scales, which is associated with a net dissipation of enstrophy. Apart from being physically desirable, the net conservation of energy and dissipation of enstrophy are important for the numerical stability of the parameterization scheme. By bounding the energy and enstrophy norms, the approach proposed here remains numerically stable despite the use of a negative viscosity. A more detailed discussion of the implications of our approach for the spectral energy and enstrophy budget, as well as for the numerical stability, is provided in [Jansen and Held \(2014\)](#).

The effect of a Laplacian viscosity on the EKE of the resolved flow can be computed as

$$\dot{E}_{\text{back}} = -\frac{1}{H} \sum_i \nu h_i |\nabla \mathbf{u}_i|^2, \quad (5)$$

where  $\nu$  is the Laplacian viscosity coefficient, which here is *negative* and controls the strength of the energy backscatter. For simplicity,  $\nu$  is assumed constant in the vertical. We will return to the choice of  $\nu$  below. Notice that there is some freedom as to how exactly the sub-grid energy source and sink terms in [Eqs. \(4\) and \(5\)](#) are formulated, with different formulations differing by contributions that can be absorbed into the flux term. The formulations chosen here have the advantage that they are Galilean invariant, the backscatter is positive definite, and there exists a certain symmetry between the hyper-viscous and backscatter terms—specifically the two terms are in phase for plane waves.

The resolved flow EKE tendencies associated with the biharmonic viscosity and backscatter are interpreted as energy exchanges with the unresolved flow, which suggests a sub-grid EKE budget equation of the form

$$\partial_t e = -\dot{E}_{\text{diss}} - \dot{E}_{\text{back}} - \frac{1}{H} \nabla \cdot \mathbf{F} - D \quad (6)$$

where  $e$  is the vertically averaged sub-grid EKE,  $\mathbf{F}$  denotes a horizontal flux of sub-grid EKE and  $D$  denotes dissipation. Recall that  $\dot{E}_{\text{diss}}$  is generally negative, from its definition in [Eq. \(4\)](#), so the first term on the right hand side acts as a source of sub-grid EKE.

For lack of a better theory for the horizontal fluxes of EKE, the latter will here be parameterized by a diffusive process:

$$\mathbf{F} = -HK_e \nabla e. \quad (7)$$

The simulations discussed in the following use  $K_e = 600 \text{ m}^2 \text{ s}^{-1}$ , which roughly corresponds to the average eddy interface height diffusivity over the baroclinically forced region, as diagnosed from the high resolution reference simulation. Simulations with different diffusivity values suggest that the dependence of the results on the exact choice of this parameter is weak.

In geostrophic turbulence energy cascades toward larger scales, thus prohibiting a direct cascade to the micro-scale, where molecular viscosity can eventually lead to dissipation (e.g. [Rhines, 1979](#)). The pathways to dissipation of mesoscale EKE in the real ocean are still being debated, but one obvious contender is frictional dissipation in the bottom boundary layer (see [Wunsch and Ferrari, 2004; Ferrari and Wunsch, 2009](#), for a review). In the present model the latter is parameterized by a quadratic bottom drag, which indeed accounts for the vast majority of the EKE dissipation in the high resolution reference simulation. [Jansen and Held \(2014\)](#) argue that the frictional dissipation of sub-grid EKE,  $D$ , is generally much smaller than  $\dot{E}_{\text{diss}}$  and  $\dot{E}_{\text{back}}$ , so that the global balance is primarily between the latter two

terms. Simulations in which  $D$  was formulated consistently with the bottom drag law applied for the resolved flow, confirm this finding, and yield very similar results to simulations in which the dissipation of sub-grid EKE was omitted. For simplicity we thus here discuss only results of simulations where  $D = 0$ .

The sub-grid EKE,  $e$ , is then used to formulate the negative viscosity coefficient for the backscatter:

$$\nu = -c_{\text{back}} \Delta \sqrt{\max(2e, 0)}, \quad (8)$$

where  $c_{\text{back}}$  is an  $O(1)$  non-dimensional constant, and  $\Delta$  is the grid scale. We choose the grid scale to set the length scale in the negative viscosity, because our aim is to parameterize energy backscatter from eddies that are just smaller than the grid scale. Since the viscous dissipation in [Eq. \(4\)](#) that acts as the source of sub-grid EKE is not strictly positive definite, [Eq. \(6\)](#) can predict negative sub-grid EKE levels at some times and locations, in which case [Eq. \(8\)](#) implies no backscatter forcing. The simulations performed in the context of this study show that such instances are generally rare and isolated, but do occur. While negative sub-grid energy is physically unsatisfying, it has no consequences for the resolved flow. [Eq. \(6\)](#) guarantees that, in the absence of sub-grid dissipation, the net sources and sinks of EKE to the resolved flow remain in balance, irrespective of the actual value of sub-grid EKE.

The energy budget constraint also leads to a relatively weak dependence of the resolved flow on the backscatter coefficient  $c_{\text{back}}$ . In a statistically steady state, the globally integrated energy backscatter ([Eq. \(5\)](#)) has to balance the integrated viscous dissipation ([Eq. \(4\)](#)). This constrains the (appropriately averaged) negative viscosity in [Eq. \(8\)](#). The primary effect of a reduction in  $c_{\text{back}}$  thus is an increase in the sub-grid EKE level, and vice-versa, without any direct consequences for the resolved flow. A secondary effect of changes in  $c_{\text{back}}$  is to modify the effective residence time of EKE at sub-grid scales, which in turn modulates the amount of horizontal spreading of EKE via the diffusive transport parameterization. As discussed above, our results are relatively insensitive to moderate changes in the sub-grid EKE transport. The backscatter coefficient was here chosen independently of the resolution as  $c_{\text{back}} = 0.4$ , which yields sub-grid EKE levels that are in rough agreement with the levels of small-scale EKE found in the high resolution reference simulation. The sensitivity of our results to the choice of  $c_{\text{back}}$  is discussed in [Section 4](#).

### 3.2. Numerical results

We start by considering the sub-grid EKE, predicted by [Eq. \(6\)](#). [Fig. 7](#) shows a snapshot as well as the time mean sub-grid EKE,  $e$ , for simulations at  $\Delta = 10 \text{ km}$ , and  $\Delta = 20 \text{ km}$  resolution with energy budget-based negative viscosity backscatter. The snapshots show a patchy pattern, dominated by a few regions with high sub-grid EKE levels, associated with strong local shears. The diffusion of sub-grid EKE acts to smooth these patches to extend over at least a few grid-points, but it does not appear to spread EKE excessively beyond dynamically connected regions. The time-mean sub-grid EKE is elevated primarily in the regions of high eddy activity. Notable exceptions are strong local maxima near the northern and southern boundaries in the vicinity of the topographic ridge. Comparison to the mean-flow pattern shows that these regions are associated with very sharp boundary currents, which lead to strong viscous dissipation, and thus here a strong source of sub-grid EKE. Whether or not the energy dissipated by viscosity in such boundary currents should be available for energy backscatter remains an open question. We will return to this issue in the discussion.

[Figs. 8 and 9](#) show the time-mean resolved EKE and mean flow for simulations with backscatter at  $\Delta = 10 \text{ km}$  and  $\Delta = 20 \text{ km}$  resolution. At a resolution of  $\Delta = 10 \text{ km}$  both the EKE and mean flow very closely resemble the results of the high resolution reference case shown in [Figs. 3 and 4](#). The results are significantly improved as

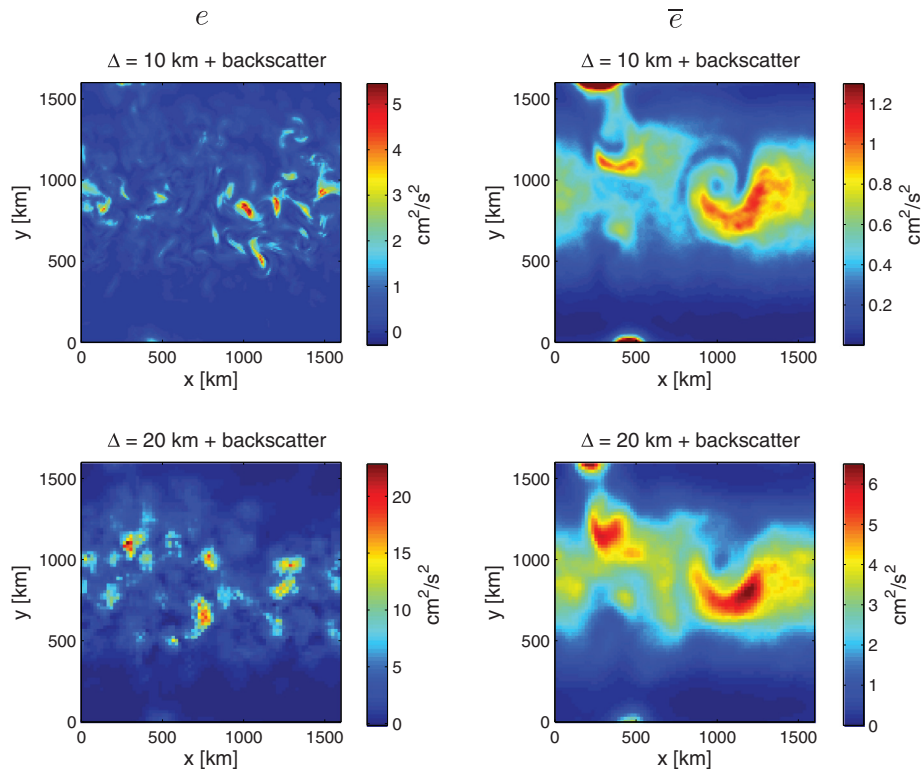


**Fig. 7.** Snapshot (left) and time-mean (right) of sub-grid EKE for simulations with negative viscosity backscatter, at 10 km (top), and 20 km (bottom) resolution. Notice that the color scale in the top right panel is saturated at the maxima.

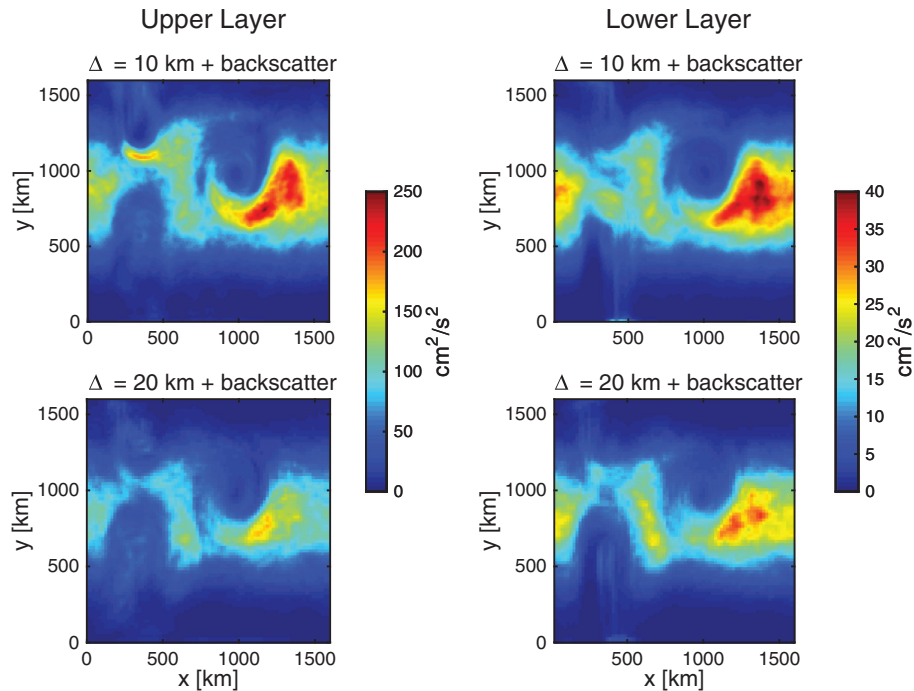


**Fig. 8.** Time-mean EKE for simulations with negative viscosity backscatter, at 10 km (top), and 20 km (bottom) resolution. The left column show the EKE in the upper layer, while the right column shows the EKE in the lower layer. The color shading is identical to Fig. 4.

compared to the simulation without backscatter, which showed significantly reduced EKE and weakened mean flows, particularly in the lower layer. At a resolution of  $\Delta = 20$  km, Figs. 8 and 9 show somewhat weakened EKE and mean flows, compared to the highest resolution reference simulation. However, the results are much improved over the simulation with similar resolution but without backscatter,

where the EKE and lower layer flow were very weak. Instead, the simulation with backscatter and  $\Delta = 20$  km shows similar levels and patterns of EKE, as well as similar mean flows, as the simulation without backscatter at  $\Delta = 10$  km resolution.

Big improvements are also found for the eddy driven overturning transport. Fig. 5 shows that the simulation with backscatter and

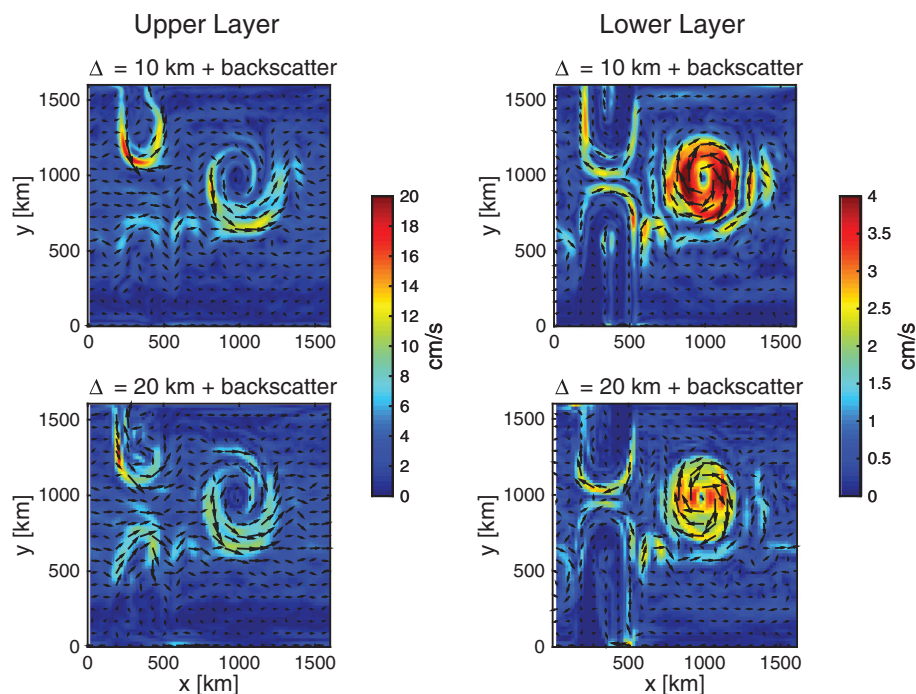


**Fig. 9.** Time-mean flow speed (shading) and direction (arrows) for simulations with negative viscosity backscatter, at 10 km (top), and 20 km (bottom) resolution. The left column show the mean flow in the upper layer, while the right column shows the mean flow in the lower layer. The color shading is identical to Fig. 3.

$\Delta = 10$  km almost perfectly reproduces the high resolution reference simulation with  $\Delta = 3.2$  km. The simulation with backscatter and  $\Delta = 20$  km again produces results similar to those obtained in the reference simulation without backscatter and  $\Delta = 10$  km. The simulations with backscatter also perform much better than the simulations without backscatter but strongly reduced bi-harmonic viscosity coefficient. The simulations with backscatter themselves are less sensitive to the choice of the bi-harmonic viscosity coefficient (not shown). This reduced sensitivity to the viscosity coefficient is an additional advantage of the backscatter formulation, which is also reported in atmospheric model results of Zurita-Gotor et al. (2015).

To further analyze the effects of backscatter on the turbulent flow, we return to the EKE spectra in Fig. 6. Away from the grid-scale, the backscatter parameterization strongly improves the EKE spectra, with the results at  $\Delta = 10$  km resolution again being almost indistinguishable from the high resolution reference simulation. The simulation with backscatter and  $\Delta = 20$  km again produces results that are similar or superior to the results obtained without backscatter at  $\Delta = 10$  km resolution. The backscatter parameterization is able to restore the energy level at the larger (most energetic) scales much more effectively than what is achieved by simply reducing the biharmonic viscosity coefficient. At the same time the energy level rolls off more steeply right above the grid-scale, which may be desirable for numerical reasons (Ilcak et al., 2012).

#### 4. Discussion

The results presented above suggest that an energy budget-based negative viscosity backscatter parameterization may be able to significantly improve ocean simulations at eddy permitting resolutions. However, while the simulations discussed above use the primitive equation dynamical core of a state-of-the-art numerical ocean model, the setup remains highly idealized, and thus avoids potential complications that need to be considered when performing global ocean simulations.

One limitation of the current formulation is associated with the potential occurrence of large Rossby number flows. While imple-

mentable in primitive equations, the closure here is derived based on physical arguments that pertain to the geostrophically balanced flow, which does dominate the dynamics in the simulations discussed here. At higher Rossby numbers, oceanic flows may become unbalanced and generate a forward cascade of energy—thus justifying viscous energy dissipation (e.g. Molemaker et al., 2010). Indeed it has been argued that loss of balance (e.g. through surface frontogenesis) may represent an important pathway to dissipation of mesoscale EKE in the ocean (Molemaker et al., 2010; Ferrari and Wunsch, 2009). We also tested the backscatter parameterization in the model configuration used by Hallberg (2013), which has a smaller Coriolis parameter and develops stronger flows, leading to larger Rossby numbers (with  $Ro \approx 1$  in strong vortices). While the backscatter parameterization in this configuration still improves the EKE level and residual transport, the improvements are smaller and some biases associated with the parameterization are also observed. While a detailed study of large Rossby number effects is beyond the scope of this study, we can offer some preliminary thoughts on how this shortcoming may be handled in global ocean models.

As mentioned above, large Rossby number flows can lead to loss of balance and eventually a forward energy cascade. Viscous energy dissipation may thus be physically desirable. This suggests a relatively simple generalization of the sub-grid EKE budget by tapering the viscous source term in the presence of high Rossby numbers. The modified sub-grid EKE variable may loosely be interpreted as representing the balanced part of the sub-grid EKE. Over most of the ocean the mesoscale eddies have small Rossby numbers,<sup>1</sup> such that this modification would likely have little effect in a typical “eddy permitting” model, outside of the equatorial region. However, at high resolution, when the model starts to explicitly resolve frontogenesis or the

<sup>1</sup> The Rossby number can easily be estimated as  $Ro \sim U/(fL)$ , where  $U$  is a characteristic flow speed and  $L$  is a characteristic length scale. With typical mesoscale eddy flow speeds of  $U \sim 0.1$  m/s and length scales  $L \sim 1 \times 10^5$  m, we find typical mid-latitude ( $f \sim 1 \times 10^{-4} \text{ s}^{-1}$ ) Rossby numbers of  $Ro \sim 1 \times 10^{-2}$ . Much larger Rossby numbers are expected in close proximity to the equator.

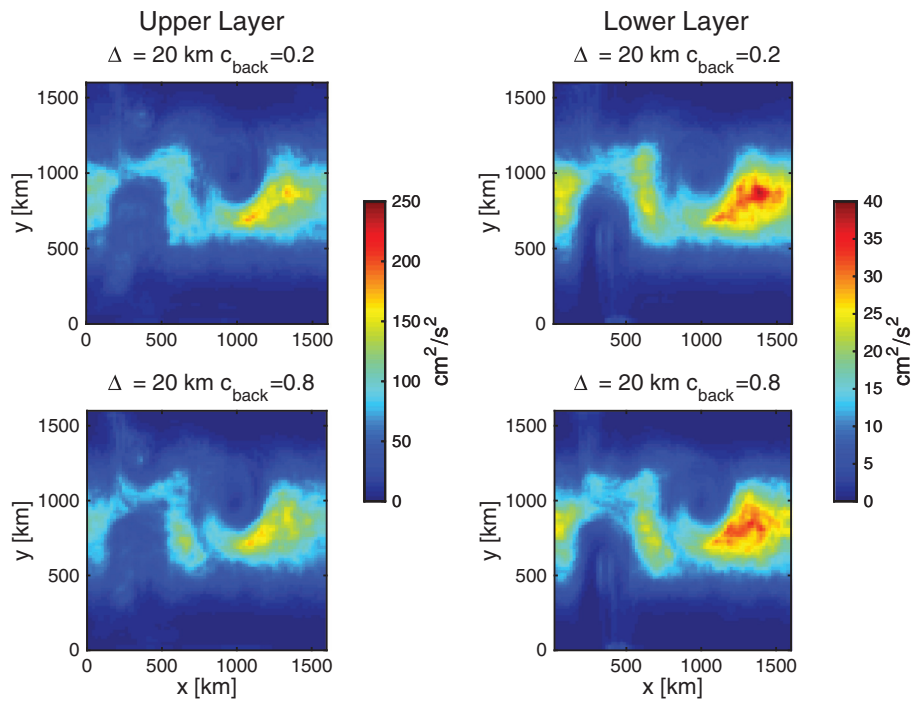


**Fig. 10.** Time-mean EKE for simulations at 20km resolution with negative viscosity backscatter, using two different values for the backscatter coefficient:  $c_{\text{back}} = 0.2$  (top) and  $c_{\text{back}} = 0.8$  (bottom). The left column shows the EKE in the upper layer, while the right column shows the EKE in the lower layer. The color shading is identical to Figs. 4 and 8.

internal wave field,<sup>2</sup> grid scale Rossby numbers may become large, and thus the backscatter parameterization would effectively get turned off. The lack of backscatter in the high resolution limit is likely to be desirable, due to the potential for a forward energy cascade, and due to the models expected ability to fully resolve the mesoscale (balanced) dynamics.

A somewhat related question pertains to the processes in boundary currents—particularly along the western boundaries. Zhai et al. (2010) argued that the western boundaries may represent a significant sink of mesoscale eddy energy. While the exact routes to dissipation remain unclear, potential candidates include the reflection of long westward propagating Rossby waves into short eastward propagating modes (e.g. Pedlosky, 1982), which represents a transfer of EKE to smaller scales and may lead to eventual dissipation via loss of balance, as well as various modes of interaction with the topography along the slope (e.g. Dewar and Hogg, 2010; Nikurashin and Ferrari, 2010). If such processes are important they may need to be included as additional loss terms in the sub-grid EKE budget. However, an adequate parameterization of sub-grid EKE loss first requires an adequate understanding of the relevant processes, which highlights the importance of further research into the pathways to dissipation of mesoscale EKE in the ocean.

For simplicity the sub-grid EKE budget was formulated only for the vertically integrated EKE, which avoids the necessity for an explicit description of vertical sub-grid energy transfers. The backscatter forcing was then accomplished using a vertically constant negative viscosity coefficient. Assuming that the spatial scales are roughly constant throughout the water column, this implies a vertical structure of the energy input that is roughly proportional to the vertical structure of EKE of the resolved flow, which seems to be a reasonable first guess. For the two-layer model analyzed in this study, this simplified description is sufficient. However, in global ocean

models, the vertical structure can become more complex, with the water column potentially containing multiple dynamically distinct regions. This may be of particular relevance at higher resolutions, when instabilities confined to the mixed layer can be explicitly resolved (Boccaletti et al., 2007). A vertically localized energy budget may then need to be considered.

It should also be noted that the parameterization proposed here is applicable only as long as the scale of baroclinic instability is at least marginally resolved. Using the current setup, simulations performed at resolutions  $\Delta = 32$  km or coarser develop no eddies, whether or not backscatter is included. When the resolution is insufficient to allow for baroclinic instability to occur, traditional parameterizations, such as proposed by Gent and McWilliams (1990) (GM), need to be employed. In global ocean simulations, where the resolution may be “eddy-permitting” in some regions, while being insufficient to generate eddies in other regions, a resolution function may be used to locally switch between a GM-type parameterization, and the backscatter parameterization proposed here (Hallberg, 2013). Alternatively, future parameterizations may combine the backscatter approach with an energy budget-based GM parameterization as proposed by Eden and Greatbatch (2008) and Jansen et al. (2015), such that both can be active simultaneously. Both routes will likely be explored in future work.

Before concluding, we would like to re-iterate that the sub-grid EKE budget employed here automatically regulates the strength of the backscatter, without relying on heavy tuning of the backscatter forcing. While the sub-grid EKE level is sensitive to the backscatter coefficient,  $c_{\text{back}}$ , the total strength of the backscatter forcing is constrained by the energy budget, such that (in a time- and spatial-average) the total energy input always equals the hyper-viscous energy dissipation. As a consequence, the effect of the backscatter forcing on the resolved flow is only weakly sensitive to the backscatter coefficient,  $c_{\text{back}}$ . This is illustrated in Fig. 10, which shows the EKE of the resolved flow in two simulations with a resolution of  $\Delta = 20$  km and with backscatter coefficients  $c_{\text{back}} = 0.2$  (i.e. half of the reference value used above) and  $c_{\text{back}} = 0.8$  (i.e. twice the reference value). In both cases, the overall strength and pattern of EKE are very similar to

<sup>2</sup> At wavelength below about 20 km, the internal wave field has kinetic energy spectra falling off with a slope near  $E(k) \sim k^{-2}$  (e.g. Callies and Ferrari, 2013, and references therein). This suggests that the shear (and thus the Rossby number) increases at small scales.

the simulation with  $c_{\text{back}} = 0.4$  discussed above (Fig. 8). Some small differences in the EKE patterns remain, and are expected due to the indirect effect of changes in  $c_{\text{back}}$  on the residence time and thus on the amount of horizontal spreading of sub-grid EKE. However, these differences are negligible compared to the overall effect of including energetically constrained backscatter (compare to Fig. 4). Notice that the weak sensitivity to  $c_{\text{back}}$  is a consequence of the negligible sub-grid EKE dissipation. In different parameter regimes, where a significant part of EKE is dissipated via a forward cascade, the results are expected to depend on the ratio of backscatter to small scale dissipation.

## 5. Summary and conclusions

A framework to parameterize sub-grid scale eddy effects in eddy permitting ocean models was discussed. The parameterization is based on previous work (Jansen and Held, 2014), which suggested to combine the typically applied bi-harmonic viscosity with a mechanism to return the spuriously dissipated energy to the resolved flow. If energy is returned at larger scales than the hyper-viscous dissipation, the result is a sub-grid closure that dissipates enstrophy while conserving (global) energy. The parameterization proposed here makes use of a predictive equation for the sub-grid EKE (Eden and Greatbatch, 2008; Jansen et al., 2015; Marshall and Adcroft, 2010). Energy dissipated by hyperviscosity acting on the resolved flow appears as a source of sub-grid EKE, while an additional forcing term transfers energy back from the sub-grid EKE to the resolved flow. This forcing term, which may loosely be interpreted as representing “backscatter” of energy from the sub-grid scales to the resolved flow (Kraichnan, 1976; Frederiksen and Davies, 1997; Kitsios et al., 2013), is formulated via a negative Laplacian viscosity.

The parameterization is tested using an idealized configuration of the GOLD primitive equation ocean model. It is shown that inclusion of the energy backscatter significantly improves the solutions of simulations at typical eddy-permitting resolutions. The parameterization helps to restore adequate EKE levels, which in turn leads to improved representations of the eddy driven overturning transport as well as eddy driven horizontal mean flows. The idealized simulations discussed here suggest the potential of the parameterization to cut the resolution required to adequately represent eddy effects in half, as compared to simulations without energy backscatter. Whether similar improvements can be achieved in global ocean models, where additional processes and complications need to be considered, remains an open question for future work. However, we are confident that significant improvements can be expected in ocean regions where eddies are important for the transport of properties and equilibration of the mean flow.

## Acknowledgements

We would like to thank Stephen Griffies, Tony Rosati, Pablo Zurita-Gotor, and two anonymous reviewers for their comments, which helped to improve the manuscript. M.F.J. acknowledges funding from a NOAA Climate and Global Change Postdoctoral Fellowship, administered by the University Corporation for Atmospheric Research. A.J.A. was supported under awards NA08OAR4320752 and NA14OAR4320106 from the National Oceanic and Atmospheric Administration, U.S. Department of Commerce. The statements, findings, conclusions, and recommendations are those of the authors and do not necessarily reflect the views of the National Oceanic and Atmospheric Administration, or the U.S. Department of Commerce.

## References

Arakawa, A., Hsu, Y.J.G., 1990. Energy conserving and potential-enstrophy dissipating schemes for the shallow water equations. *Mon. Wea. Rev.* 118, 1960–1969.

- Berloff, P., 2015. Dynamically consistent parameterization of mesoscale eddies. Part I: Simple model. *Ocean Modell.* 87, 1–19.
- Boccaletti, G., Ferrari, R., Fox-Kemper, B., 2007. Mixed layer instabilities and restratification. *J. Phys. Oceanogr.* 37 (9), 2228–2250.
- Böning, C.W., Budich, R.G., 1992. Eddy dynamics in a primitive equation model: Sensitivity to horizontal resolution and friction. *J. Phys. Oceanogr.* 22, 361–381.
- Bretherton, F.P., Haidvogel, D.B., 1976. Two-dimensional turbulence above topography. *J. Fluid Mech.* 78, 129–154.
- Callies, J., Ferrari, R., 2013. Interpreting energy and tracer spectra of upper-ocean turbulence in the submesoscale range (1–200 km). *J. Phys. Oceanogr.* 43 (11), 2456–2474.
- Cessi, P., 2008. An energy-constrained parameterization of eddy buoyancy flux. *J. Phys. Oceanogr.* 38, 1807–1819.
- Charney, J.G., 1971. Geostrophic turbulence. *J. Atmos. Sci.* 28, 1087–1094.
- Dewar, W.K., Hogg, A.M., 2010. Topographic inviscid dissipation of balanced flow. *Ocean Modell.* 32 (1–2), 1–13. The magic of modelling: A special volume commemorating the contributions of Peter D. Killworth—Part I.
- Duan, J., Nadiga, B.T., 2007. Stochastic parameterization for large eddy simulation of geophysical flows. *Proc. Amer. Math. Soc.* 135, 1187–1196.
- Eden, C., Greatbatch, R.J., 2008. Towards a mesoscale eddy closure. *Ocean Modell.* 20 (3), 223–239.
- Ferrari, R., Wunsch, C., 2009. Ocean circulation kinetic energy—Reservoirs, sources and sinks. *Ann. Rev. Fluid Mech.* 41, 253–282.
- Flato, G., Marotzke, J., Abiodun, B., Braconnot, P., Chou, S., Collins, W., Cox, P., et al., 2013. Evaluation of climate models. In: Stocker, T., Qin, D., Plattner, G.K., Tignor, M., Allen, S., Boschung, J., Nauels, A., Xia, Y., Bex, V., Midgley, P. (Eds.), *Climate Change 2013: The Physical Science Basis. Contribution of Working Group I to the Fifth Assessment Report of the Intergovernmental Panel on Climate Change*. Cambridge University Press, Cambridge, UK and New York, NY, USA, pp. 741–866.
- Fox-Kemper, B., Menemenlis, D., 2008. Can large eddy simulation techniques improve mesoscale rich ocean models?. In: Hecht, M.W., Hasumi, H. (Eds.) *Ocean Modelling in an Eddy Regime*, vol. 177. American Geophysical Union, Washington, DC, pp. 319–337. doi:10.1029/177GM19.
- Frederiksen, J.S., Davies, A.G., 1997. Eddy viscosity and stochastic backscatter parameterizations on the sphere for atmospheric circulation models. *J. Atmos. Sci.* 54, 2475–2492.
- Galperin, B., Sukoriansky, S., Orszag, S.A., Staroselsky, I., 1993. Non-eddy resolving model of  $\beta$ -plane turbulence. In: *Statistical Methods in Physical Oceanography: Proceedings 'Aha Huli' Hawaiian Winter Workshop*, University of Hawaii at Manoa, January 12–15, 1993, pp. 421–452.
- Gent, P.R., McWilliams, J.C., 1990. Isopycnal mixing in ocean circulation models. *J. Phys. Oceanogr.* 20, 150–155.
- Gent, P.R., Willebrand, J., McDougall, T.J., McWilliams, J.C., 1995. Parameterizing eddy-induced tracer transports in ocean circulation models. *J. Phys. Oceanogr.* 25, 463–474.
- Gill, A.E., Green, J.S.A., Simmons, A.J., 1974. Energy partition in the large-scale ocean circulation and the production of mid-ocean eddies. *Deep Sea Res.* 21 (7), 499–528.
- Greatbatch, R.J., Li, G., 2000. Alongslope mean flow and an associated upslope bolus flux of tracer in a parameterization of mesoscale turbulence. *Deep Sea Res. I: Oceanog. Res. Papers* 47 (4), 709–735.
- Griffies, S.M., 2004. *Fundamentals of Ocean Climate Models*. Princeton University Press.
- Griffies, S.M., Halberg, R., 2000. Biharmonic friction with a Smagorinsky-like viscosity for use in large-scale eddy-permitting ocean models. *Mon. Wea. Rev.* 128, 2935–2946.
- Griffies, S.M., Winton, M., Anderson, W.G., Benson, R., Delworth, T.L., Dufour, C.O., Dunne, J.P., et al., 2015. Impacts on ocean heat from transient mesoscale eddies in a hierarchy of climate models. *J. Climate* 28 (3), 952–977.
- Grooms, I., Majda, A.J., Smith, K.S., 2015. Stochastic superparameterization in a quasi-geostrophic model of the antarctic circumpolar current. *Ocean Modell.* 85, 1–15.
- Hallberg, R., 2013. Using a resolution function to regulate parameterizations of oceanic mesoscale eddy effects. *Ocean Modell.* 72, 92–103.
- Hallberg, R., Adcroft, A., 2009. Reconciling estimates of the free surface height in lagrangian vertical coordinate ocean models with mode-split time stepping. *Ocean Modell.* 29 (1), 15–26.
- Hallberg, R., Gnanadesikan, A., 2006. The role of eddies in determining the structure and response of the wind-driven southern hemisphere overturning: Results from the modeling eddies in the Southern Ocean (MESO) project. *J. Phys. Oceanogr.* 36 (12), 2232–2252.
- Holloway, G., 1992. Representing topographic stress for large-scale ocean models. *J. Phys. Oceanogr.* 22, 1033–1046.
- Ilcak, M., Adcroft, A.J., Griffies, S.M., Hallberg, R.W., 2012. Spurious diurnal mixing and the role of momentum closure. *Ocean Modell.* 45, 37–58.
- Jansen, M.F., Adcroft, A.J., Hallberg, R., Held, I.M., 2015. Parameterization of eddy fluxes based on a mesoscale energy budget. *Ocean Modell.* 92, 28–41.
- Jansen, M.F., Held, I.M., 2014. Parameterizing subgrid-scale eddy effects using energetically consistent backscatter. *Ocean Modell.* 80, 36–48.
- Johnson, G.C., Bryden, H.L., 1989. On the size of the antarctic circumpolar current. *Deep Sea Res. A. Oceanog. Res. Papers* 36 (1), 39–53.
- Kitsios, V., Frederiksen, J., Zidikheri, M., 2013. Scaling laws for parameterisations of sub-grid eddy-eddy interactions in simulations of oceanic circulations. *Ocean Modell.* 68, 88–105.
- Kraichnan, R.H., 1976. Eddy viscosity in two and three dimensions. *J. Atmos. Sci.* 33, 1521–1536.

- Larichev, V.D., Held, I.M., 1995. Eddy amplitudes and fluxes in a homogeneous model of fully developed baroclinic instability. *J. Phys. Oceanogr.* 25, 2285–2297.
- Leith, C., 1990. Stochastic backscatter in a subgrid-scale model: Plane shear mixing layer. *Phys. Fluids A* 2, 297–299.
- Marshall, D.P., Adcroft, A.J., 2010. Parameterization of ocean eddies: Potential vorticity mixing, energetics and Arnold's first stability theorem. *Ocean Modell.* 32 (3–4), 188–204. The magic of modelling: A special volume commemorating the contributions of Peter D. Killworth—Part 2.
- McWilliams, J.C., 2008. The nature and consequences of oceanic eddies. In: *Geophysical Monograph Series*, vol. 177. American Geophysical Union, Washington, DC, pp. 5–15.
- Molemaker, M.J., McWilliams, J.C., Capet, X., 2010. Balanced and unbalanced routes to dissipation in an equilibrated eady flow. *J. Fluid Mech.* 654, 35–63.
- Nikurashin, M., Ferrari, R., 2010. Radiation and dissipation of internal waves generated by geostrophic motions impinging on small-scale topography: Theory. *J. Phys. Oceanogr.* 40 (5), 1055–1074.
- Oschlies, A., 2002. Improved representation of upper-ocean dynamics and mixed layer depths in a model of the North Atlantic on switching from eddy-permitting to eddy-resolving grid resolution. *J. Phys. Oceanogr.* 32, 2277–2298.
- Pedlosky, J., 1982. *Geophysical Fluid Dynamics*. Springer-Verlag, New York and Berlin.
- Rhines, P.B., 1977. The dynamics of unsteady currents. In: Goldberg, E. (Ed.), *The Sea*, VI. John Wiley and Sons, Inc., NY, pp. 189–318.
- Rhines, P.B., 1979. Geostrophic turbulence. *Annu. Rev. Fluid Mech.* 11, 401–441.
- Salmon, R., 1978. Two-layer quasi-geostrophic turbulence in a simple special case. *Geophys. Astrophys. Fluid Dyn.* 10 (1), 25–52.
- Smagorinsky, J., 1963. General circulation experiments with the primitive equations. *Mon. Wea. Rev.* 91, 99–164.
- Talley, L., 2013. Closure of the global overturning circulation through the Indian, Pacific, and southern oceans: Schematics and transports. *Oceanography* 26 (1), 80–97.
- Thuburn, J., Kent, J., Wood, N., 2014. Cascades, backscatter and conservation in numerical models of two-dimensional turbulence. *Q. J. Roy. Meteor. Soc.* 140, 626–638.
- Tulloch, R., Ferrari, R., Jahn, O., Klocker, A., Lacasce, J., Ledwell, J., Marshall, J., et al., 2014. Direct estimate of lateral eddy diffusivity upstream of Drake passage. *J. Phys. Oceanogr.* 44 (10), 2593–2616.
- Waterman, S., Hogg, N.G., Jayne, S.R., 2011. Eddy-mean flow interaction in the Kuroshio extension region. *J. Phys. Oceanogr.* 41, 1182–1208.
- Wunsch, C., Ferrari, R., 2004. Vertical mixing, energy, and the general circulation of the oceans. *Annu. Rev. Fluid Mech.* 36, 281–314.
- Zhai, X., Johnson, H.L., Marshall, D.P., 2010. Significant sink of ocean-eddy energy near western boundaries. *Nat. Geosci.* 3 (9), 608–612.
- Zurita-Gotor, P., Held, I.M., Jansen, M.F., 2015. Kinetic energy-conserving hyperdiffusion can improve low resolution atmospheric models. *J. Adv. Model. Earth Syst.* 07. doi:10.1002/2015MS000480.